field of frequency c/λ), we expect to obtain a pretty good approximate description by replacing all periodic functions of the time (possessing the smaller period $\tau_0 \equiv a/c$) by their respective time averages over any time interval of duration a/c. It should be emphasized, however, that this approximation will become worse and worse as $\lambda \to a$.[11]

In conclusion, we wish to reiterate that by making the *single* approximation of replacing the coefficients $V(\mathbf{r})-\bar{V}(x,y)$ and $-i(e/m)(\partial/\partial x)\ln u_k(x,y)$ in Eq. (21) by their respective averages over any single lattice cell, we have succeeded in reducing our original problem to an ordinary second-order differential equation in the single independent variable ξ, and this differential equation can now be easily solved to essentially any desired degree of accuracy. On the other hand, more conventional approaches to a theoretical description of the interaction of laser radiation with electrons in solids frequently resort to one or more of the following approximations (in addition to the one-electron approximation which we assumed from the very beginning):

(1) The spatial variation of the electromagnetic field is usually neglected, i.e., $\mathbf{A}(\xi)$ is replaced by $\mathbf{A}(-t)$. This amounts to complete neglect of the linear momentum associated with the electromagnetic field.

(2) The effects produced by H_{int} are calculated by using ordinary time-dependent perturbation theory—even though the effective coupling constant is not necessarily small compared to unity.

(3) With regard to the use of time-dependent perturbation theory, the unperturbed electron state is usually assumed to be described by the effective mass approximation, i.e., H_0 is replaced by $(\mathbf{p}^2/2m^*)$, where m^* denotes the so-called effective mass.

These three examples of typical approximations are cited here mainly to suggest that in certain physical situations (to be discussed more thoroughly in a subsequent article) it may be more suitable to use the formalism described here, whose validity is believed to depend on the single restriction, $\lambda \gg a$.

The author wishes to thank Professor C. Lanczos and Professor Y. Takahashi for helpful and enlightening discussions of this work. Also he wishes to thank Professor J. L. Synge for his kind hospitality at the Dublin Institute for Advanced Studies.

[11] The well-known appearance of resonance phenomena in similar situations when the driving frequency approaches the natural frequency of the driven system suggests that interesting new physical phenomena might be discovered if and when a practical γ-ray maser (producing relatively intense, coherent, and essentially monochromatic radiation of wavelength equal to the crystal lattice spacing) is developed.

PHYSICAL REVIEW VOLUME 160, NUMBER 3 15 AUGUST 1967

Self-Consistent-Field Model of Bimetallic Interfaces. I. Dipole Effects

ALAN J. BENNETT AND C. B. DUKE
General Electric Research and Development Center, Schenectady, New York

(Received 15 March 1967)

An electron-gas model of a bimetallic interface is constructed by joining two semi-infinite half-planes of unequal positive charge and adding electrons until a charge-neutral system is achieved. The electrostatic (dipole) potential equalizes the Fermi energies of the high- and low-density components of the junction by compensating for the difference in their (bulk) exchange and correlation separation energies. The model is used to calculate self-consistently the charge density and one-electron (junction) potential in the region near the interface. The barrier height V_b associated with the self-consistent potential is *not* related to the vacuum work functions ϕ_L and ϕ_R of the two-component metals by $V_b=\phi_L-\phi_R$. This result is due not to either real or "virtual" surface states, but rather to the redistribution of the electronic charge at the bimetallic interface relative to the vacuum interfaces of the separate metals. Localized "surface states" can occur for certain junction potentials on the high-density side of the interface. These states do not occur in the self-consistent potential for the numerical example of $n_L=10^{22}$ and $n_R=10^{21}$ cm^{-3}. In addition, $V_b \neq \phi_L-\phi_R$ for these positive charge densities. Although the electron density exhibits Friedel oscillations on both sides of the junction, only two of the oscillations on each side are explicitly incorporated into the model charge density used in the self-consistent loops. A semiclassical (Schottky) model of the depletion region on the low-density side of the interface is inadequate because of the presence of large evanescent contributions to the electron density.

I. INTRODUCTION

DESPITE the extensive literature on semiphenomenological models of bimetallic and metal-semiconductor interfaces,[1] little attention has been devoted to the more fundamental problems of the dynamical origin of the charge distribution near an interface and the stability of this distribution. These

[1] See, e.g., E. Spenke, *Electronic Semiconductors* (McGraw-Hill Book Company Inc., New York, 1958), Chaps. 4 and 10; D. V. Geppert, A. M. Cowley, and B. V. Dore, J. Appl. Phys. **37**, 2458 (1966).

problems are the analogs at a surface of the calculation of the cohesive energy of a self-binding system. The many-body systems for which the cohesive energy has been most extensively studied are the electron gas in a uniform positive background and nuclear matter. The analysis of the cohesion of a uniform electron gas provides the foundation for the original models,[2,3] and their later refinements,[4–6] of metallic interfaces. The calculations[2–6] of charge densities and one-electron potentials at interfaces constitute a relatively simple special case of the problem of determining the properties of an inhomogeneous many-body system[7] in which the deviations from homogeneity are in general neither small (i.e., linearizable) nor slowly varying. In order to utilize the results of previous investigations of the uniform electron gas and its vacuum interface, we adopt the model of a bimetallic interface in which the interface is specified by joining at $x=0$ two semi-infinite half-planes of (unequal) uniform positive charge. Superposed on this positive charge is an electron gas of a composition which guarantees electrical neutrality of the final system. The eigenfunctions and eigenvalues of the system are calculated self-consistently from the Poisson and Schrödinger equations and used to evaluate the charge density and one-electron ("junction") potential near the interface. The only parameters in the model are the two semi-infinite positive-charge densities. In particular, there are no phenomenological parameters like work functions, electron affinities, or energy-band gaps. Our primary interest lies in examining the qualitative character of the charge density and junction potential predicted by this highly idealized but "first-principles" model. The model can be extended easily to give a description of the (often conflicting) experimental data[8] on metal-semiconductor contacts only at the expense of introducing at least two phenomenological parameters, the electron affinity and energy gap of the semiconductor. The neglect of the periodic ionic potential, which renders the model inadequate for the description of low-energy electrons in a semiconductor without the use of additional parameters characterizing the bulk band structure, is rigorously justifiable in bimetallic junctions only in the sense of a pseudopotential[9] or extended effective-mass[10] (Bethe-Sommerfeld) approximation.

From our study of this simple electron-gas model emerge two major conclusions which are not properly incorporated in current versions[1,8] of phenomenological models of contacts. First, the redistribution of charge near a bimetallic junction relative to its distribution at the vacuum interface of either component metal implies that to within energies ~ 0.5 eV there is no general relation between the maximum height V_b of the junction potential and the difference in the vacuum work functions ϕ_L and ϕ_R of the composite metals. In particular, the failure of the equation

$$V_b=\phi_L-\phi_R; \quad \phi_L>\phi_R \tag{1.1}$$

is not in general due to conventional[11] surface states but rather is primarily a consequence of the tunneling of electrons from the high- into the low-density electron gas. Such evanescent contributions to the charge density are the electron-gas analog of Heine's "virtual" surface states[12] at a metal-semiconductor interface. In our model these contributions to the charge density are included in the self-consistent determination of the junction potential and one-electron eigenstates. However, in Heine's analysis the band bending induced by the "virtual"-surface-state contribution to the charge density modifies his starting potential and consequently invalidates conclusions based on the use of the starting potential.[13] Our second major result is that *bona fide* "localized" states near the interface can occur for suitable junction potentials. These states are concentrated on the high-density side of the interface and are the direct analog of quantized states in narrow accumulation or inversion channels at semiconductor interfaces.[14–18] Their presence is signalled not by the failure of Eq. (1.1), but rather by the failure of charge neutrality and by a qualitative change in the character of the charge distribution near the interface if their contribution to the charge density is ignored. However, we have not found a set of parameters for which these localized states occur in the final "self-consistent" junction potential.

The physical origin of the above conclusions can be demonstrated easily without appeal to a detailed analysis.[3] Measuring energies in Hartrees, we recall that for a uniform electron gas[19] of density n, and Bohr radius a_B, the Fermi energy E_F, the average kinetic

[2] E. Wigner and J. Bardeen, Phys. Rev. **48**, 84 (1935); J. Bardeen, *ibid*, **49**, 653 (1936); Surface Sci. **2**, 381 (1964).
[3] H. Y. Fan, Phys. Rev. **61**, 365 (1942); **62**, 388 (1942).
[4] H. J. Juretschke, Phys. Rev. **92**, 1140 (1953).
[5] T. L. Loucks and P. H. Cutler, J. Phys. Chem. Solids **25**, 105 (1964).
[6] M. Kaplit, in *Proceedings of the Thirteenth Field-Emission Symposium* (Cornell University, Ithaca, New York, 1966), p. 5.
[7] See, e.g., P. Hohenberg and W. Kohn, Phys. Rev. **136**, B864 (1964); W. Kohn and L. J. Sham, *ibid.* **140**, A1133 (1965).
[8] See, e.g., D. V. Geppert, A. M. Cowley, and B. V. Dore, J. Appl. Phys. **37**, 2458 (1966); A. M. Cowley and S. M. Sze, *ibid.* **36**, 3212 (1965).
[9] W. A. Harrison, *Pseudopotentials in the Theory of Metals* (W. A. Benjamin, Inc., New York, 1966).
[10] D. J. BenDaniel and C. B. Duke, Phys. Rev. **152**, 683 (1966).
[11] See, e.g., A. Many, Y. Goldstein, and N. B. Grover, *Semiconductor Surfaces* (North-Holland Publishing Company, Amsterdam, 1965), Chap. 5.
[12] V. Heine, Phys. Rev. **138**, A1689 (1965).
[13] This fact is recognized in Ref. 12, but no effort is made to extend the considerations presented therein to systematically incorporate the effects of the band bending.
[14] P. Handler and S. Eisenhour, Surface Sci. **2**, 64 (1964).
[15] F. F. Fang and W. E. Howard, Phys. Rev. Letters **16**, 797 (1966).
[16] A. B. Fowler, F. F. Fang, W. E. Howard, and P. J. Stiles, Phys. Rev. Letters **16**, 901 (1966).
[17] D. J. BenDaniel and C. B. Duke (to be published).
[18] C. B. Duke (to be published).
[19] See, e.g., P. Nozieres and D. Pines, Phys. Rev. **111**, 442 (1958).

energy $T_{\rm av}$, the exchange and correlation energy per electron $\epsilon_{\rm ec}$, and the effective single-particle exchange and correlation potential[7] $V_{\rm ec}$ are given by

$$E_F=1.84/r_s^2, \quad T_{\rm av}=0.6\,E_F, \tag{1.2a}$$

$$\epsilon_{\rm ec}=-0.458/r_s-0.44/(r_s+7.8), \tag{1.2b}$$

$$V_{\rm ec}=-\frac{0.610}{r_s}-\frac{0.44}{(r_s+7.8)}\left[1+\frac{0.33r_s}{(r_s+7.8)}\right], \tag{1.2c}$$

$$r_s=(3/4\pi a_B{}^3 n)^{1/3}. \tag{1.2d}$$

In Eqs. (1.2b) and (1.2c) we use Wigner's interpolation formula[20] for the correlation energy. The major contribution[2] to the metal-vacuum work function for a semi-infinite free-electron gas is the bulk separation energy of the electron gas

$$S_n\equiv V_{\rm ec}+E_F \tag{1.3}$$

on which is superposed an additional dipole contribution due to that (evanescent) electron contribution to the charge density which extends beyond the termination of the positive background. The dependence on the bulk electron density n of the energy $E_T=na_B{}^3(T_{\rm av}+\epsilon_{\rm ec})$, of

TABLE I. Energies associated with electrically neutral uniform electron gases of density 10^{22} cm^{-3} and 10^{21} cm^{-3}, respectively.

	$n=10^{22}$ cm^{-3}	$n=10^{21}$ cm^{-3}
E_F	1.70 eV	0.36 eV
E_T/N	−2.18 eV	−1.46 eV
$V_{\rm ec}$	−4.10 eV	−2.15 eV
S_n	−2.40 eV	−1.79 eV

the binding energy per particle $E_T/na_B{}^3$, and of the separation energy is shown in Fig. 1. These curves describe a charge-neutral system, so that the electron density n is determined by the uniform positive background rather than the saturation condition on E_T.

Several observations about Fig. 1 are significant. First, we see that for $n\lesssim 10^{22}$, $|S_n|$ is a monotonically increasing function of density. The values in electron volts of the various energies are given in Table I for uniform electron gases of densities 10^{22} and 10^{21} cm^{-3}, respectively. For both systems $S_n\sim -2$ eV and the additional dipole contribution to the vacuum work function is estimated[3] to be $\lesssim -0.5$ eV and therefore smaller than the bulk contributions by a factor of 4. However, the difference in S_n between the two systems is only $\Delta S_n=-0.6$ eV which is the same size as the dipole contributions to each separately. Hence we anticipate that dipole effects play a far more important role in determining bimetallic junction potentials than they do in determining vacuum work functions. This observation motivates the main approximation employed in this paper: The bulk exchange-correlation potential

[20] E. P. Wigner, Phys. Rev. 46, 1002 (1934).

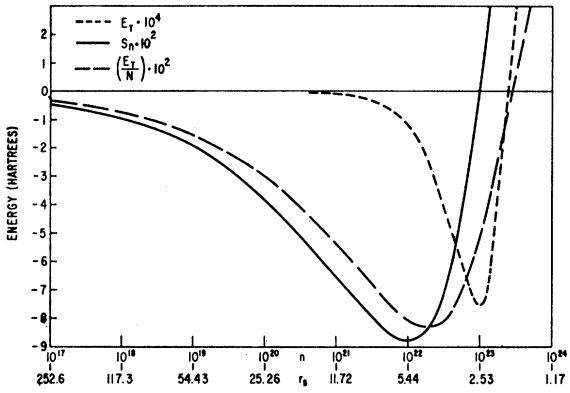

FIG. 1. The separation energy S_n, total binding energy E_T, and binding energy per particle of a uniform electron gas as a function of electron density.

$V_{\rm ec}$ is used on each side of the interface with a concommitant discontinuous change at $x=0$. We evaluate the self-consistent dipole potential which results from this simple treatment of $V_{\rm ec}$ and in a subsequent paper investigate the effect on this dipole field of various more refined treatments[4,5,7] of the exchange and correlation energies.

Using the model in which $V_{\rm ec}$ is taken to be its bulk value, we can demonstrate easily the qualitative features of the final self-consistent junction potential. From Fig. 1 we see that for metallic densities ($n\gtrsim 10^{22}$ cm^{-3}) the sign of the change in $V_{\rm ec}$ from the higher- to the lower-density metal depends sensitively on the actual densities involved. In Fig. 2 is illustrated the case which provides the most severe test of the model: A junction in which the lower-density metal exhibits a smaller bulk binding energy. The lower value of $|S_n|$ in the low-density metal, combined with the requirement that the Fermi levels equalize, leads to a dipole layer at the interface in the opposite sense to that at the metal-vacuum interface for the high-density metal. Evidently

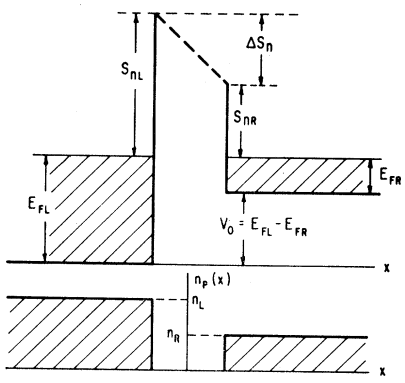

FIG. 2. A schematic representation of the positive background charge density and a conventional energy-level diagram for two metals separated by a thin vacuum layer. The figure is drawn for the case in which the lower-density metal exhibits an electron separation energy which is smaller in magnitude than that of the higher-density metal.

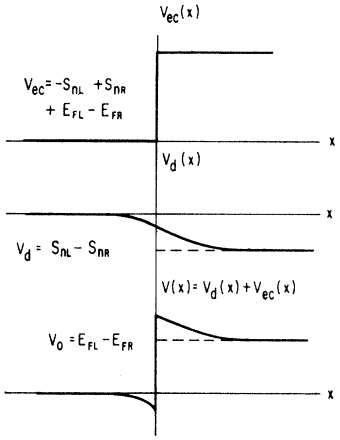

FIG. 3. A schematic representation of the bulk exchange and correlation potential V_{ec}, dipole potential V_d, and total potential in the neighborhood of a bimetallic interface at which the lower-density metal also exhibits a smaller magnitude $|S_n|$ of the electron separation energy than the higher-density metal.

a dipole potential of height $V_d=|\Delta S_n|=|S_{nR}-S_{nL}|$ must be generated near the interface. The details of the junction potential depend upon how this potential drop is divided between the two metals. Therefore all that can be said, *a priori*, about the maximum height of the junction potential V_b is that it probably satisfies

$$V_b \leq V_d = S_{nR} - S_{nL} \tag{1.4}$$

with the equality holding for a (Schottky) barrier in which the entire voltage drop occurs across the low-density metal. Even in this case it is the difference in the bulk separation energies, not the observed work functions, which appears in Eq. (1.4) as opposed to Eq. (1.1). A schematic representation of the junction potential is shown in Fig. 3. Evidently a (Schottky) depletion region is probable if $V_d > E_{FR}$ and occurs only if $V_{\max} - V_0 > E_{FR}$. The dip in the potential on the left-hand side near $x=0$ can, in some cases, contain one or more bound states which are the "localized" states referred to above. The occurrence of such states requires simultaneously a large V_d and a sufficiently long range on the left-hand side (i.e., low-continuum charge density). The density parameters, $n_L=10^{22}$ cm^{-3} and $n_R=10^{21}$ cm^{-3} (for which the results of detailed numerical calculations are given in subsequent sections) represent a limiting case of the model in which localized states might be expected to occur on the high-density side of the junction at actual metallic densities. Even in this limit, however, such states do not occur in the self-consistent potential.

From the above discussion we see that the general features, although not the details, of our results are self-evident from simple physical considerations.[3] The body of this paper is devoted to making these considerations quantitative. In Sec. II we outline the self-consistent-field boundary-value problem and investigate the quantum-theory charge density resulting from two model potentials $V(x)$ for which the Schrödinger equation can be solved analytically. From the characteristic features of these model charge densities we select, in Sec. III, a four-region parametrized model of the charge density for use in the full self-consistent-field calculation. The remainder of Sec. III is devoted to the specification of the details of the self-consistent calculation, together with a presentation and discussion of the results of this calculation.

II. CALCULATION OF THE CHARGE DENSITY

A. Definition of the Boundary-Value Problem

The boundary-value problem which we consider is that of obtaining the (one-electron) dipole potential $V_d(x)$ defined to be the solution of Poisson's equation

$$\frac{d^2V_d}{dx^2}=\frac{4\pi e^2}{\epsilon}n(x), \tag{2.1a}$$

$$n(x)=n_p(x)-n_e(x) \tag{2.1b}$$

for a system of interacting electrons in a positive background given by

$$n_p(x)=n_L\Theta(-x)+n_R\Theta(x), \tag{2.2}$$

$$\Theta(x)=+1; \quad x>0$$
$$=\ 0; \quad x<0. \tag{2.3}$$

The electrons are taken to interact through Coulomb interactions with the resultant exchange and correlation energy for a uniform system given in the Introduction. The Hartree Coulomb energy of the inhomogeneous system is obtained from the one-electron potential $V_d(x)$ specified by Eq. (2.1). The total system is required to be electrically neutral in the sense that

$$\int_{-\infty}^{+\infty}[n_p(x)-n_e(x)]dx=0. \tag{2.4}$$

The electron density $n_e(x)$ is obtained by solving the Schrödinger equation

$$\left[-\frac{\hbar^2}{2m}\frac{d^2}{dx^2}+V(x)-E_x\right]\psi_{E_x}(x)=0, \tag{2.5a}$$

$$V(x)=V_d(x)+V_{ec}(x), \tag{2.5b}$$

$$\psi(r)=\frac{\exp(i\mathbf{k}_{||}\cdot\boldsymbol{\varrho})}{2\pi}\psi_{E_x}(x), \tag{2.5c}$$

$$E=(\hbar^2k_{||}^2/2m_{||})+E_x \tag{2.5d}$$

and filling all states (at zero temperature) below a chemical potential, $\mu\equiv E_{FL}=\hbar^2k_{FL}^2/2m$, defined such

that Eq. (2.4) is satisfied. We use

$$n(x)=n_c(x)+n_{ss}(x),$$

$$n_c(x)=\frac{(2s+1)}{2\pi}\frac{m_{||}}{\hbar^2} \tag{2.6a}$$

$$\times\sum_i\int_0^\mu |\psi_{E_x}{}^{(i)}(x)|^2(\mu-E_x)dE_x, \tag{2.6b}$$

$$E_x\equiv\hbar^2k_x{}^2/2m_\perp, \tag{2.6c}$$

$$n_{ss}(x)=\frac{(2s+1)}{2\pi}\frac{m_{||}}{\hbar^2}\sum_b(\mu+E_b)|\psi_{E_b}(x)|^2, \tag{2.6d}$$

$$\int_{-\infty}^{+\infty}\psi_{E_x}{}^{(i)}(x)\psi_{E'x}{}^{(i)}(x)dx=\delta(E_x-E_x'), \tag{2.7a}$$

$$\int_{-\infty}^{+\infty}\psi_{E_b}(x)\psi_{E'b}(x)dx=\delta_{E_b,E'b}. \tag{2.7b}$$

The n_c and n_{ss} label contributions to the electron density from the continuum and bound-state eigenvalue spectra, respectively of Eq. (2.5a). The source of these two types of spectra is the potential shown in Fig. 3. As discussed in the Introduction, our use of the bulk values for the exchange-correlation potential $V_{ec}(x)$ constitutes the major approximation of the analysis reported herein. The removal of this restriction allowing both local density expansion[7] and momentum-dependent[2-5] potentials will be described in a subsequent work. The bound-state spectrum, which creates two-dimensional bands of "surface states"[17,18] arises from the dip in the total potential on the left-hand side near $x=0$. For $E>V_0$ the continuum spectrum is doubly degenerate and the (i) labels in (2.6) indicate the (two) linearly independent eigenfunctions needed to specify the density. Continuum normalization is used throughout to avoid ambiguities which arise upon taking the infinite-system limit of box-normalized wave functions.

The self-consistent determination of the $V_d(x)$ occurring in both (2.1) and (2.5b) is achieved by the following sequence of operations: (1) Select a model $V_d(x)$ and solve Schrödinger's equation (2.5a) to obtain the density via Eqs. (2.6). (2) Parametrize the total density by a model density $n_M(x)$ which explicitly satisfies charge neutrality, Eq. (2.4), and which gives a net step size between the two media[3] of $V_0=E_{FL}-E_{FR}$; $E_{Fi}=\hbar^2k_{Fi}{}^2/2m$. [See Fig. 3]. (3) Solve Eq. (2.1) for the model charge density, $n(x)\equiv n_M(x)$ and (4) Use the $V_d(x)$ resulting from step (3) back in step (1) and repeat the loop until the parameters in $n_M(x)$ change by less then a prescribed amount upon successive iterations. The remaining three parts of Sec. II are devoted to an explanation of the details of step (1). A thorough discussion of steps (2)–(4) is given in Sec. III.

B. General Calculation of the Charge Density

The eigenfunctions of a potential such as that shown in Fig. 3 are calculated separately for the three regions $E>V_0$, $0<E<V_0$, and $E<0$, respectively. The eigenvalues $E=-E_b$ in the $E<0$ discrete spectrum are determined by the normalizability criteria as $x\to\pm\infty$, and are discussed further in those special cases in which they occur. The basic linearly independent solutions to the Schrödinger equation are taken to be the one-dimension analog of the Jost functions[21,22] defined by the boundary conditions

$$\phi_{L\pm}(x)\overset{x\to-\infty}{\longrightarrow}e^{\pm ik_Lx};\quad E_x>0 \tag{2.8a}$$
$$\longrightarrow e^{\mp q_Lx};\quad E_x<0,$$

$$E_x=\hbar^2k_L{}^2/2m_\perp;\quad E_x>0 \tag{2.8b}$$

$$E_x=-\hbar^2q_L{}^2/2m_\perp;\quad E_x<0; \tag{2.8c}$$

$$\phi_{R\pm}(x)\overset{x\to\infty}{\longrightarrow}e^{\pm ik_Rx};\quad E_x>V_0 \tag{2.9a}$$
$$\longrightarrow e^{\mp q_Rx};\quad E_x<V_0,$$

$$E_x-V_0=\hbar^2k_R{}^2/2m_\perp;\quad E_x>V_0 \tag{2.9b}$$

$$V_0-E_x=\hbar^2q_R{}^2/2m_\perp;\quad E_x<V_0. \tag{2.9c}$$

The two linearly-independent wave functions for $E_x>V_0$ are taken to be

$$\psi^{(1)}(x)=(2\pi\hbar v_L)^{-1/2}[\phi_{L+}(x)+u_{11}\phi_{L-}(x)];\quad x<0 \tag{2.10a}$$
$$=(2\pi\hbar v_R)^{-1/2}u_{21}\phi_{R+}(x);\quad x>0,$$

$$\psi^{(2)}(x)=(2\pi\hbar v_L)^{-1/2}u_{12}\phi_{L-}(x);\quad x<0 \tag{2.10b}$$
$$=(2\pi\hbar v_R)^{-1/2}[\phi_{R-}(x)+u_{22}\phi_{R+}(x)];\quad x>0$$

$$v_L=\hbar k_L/m_\perp, \tag{2.11a}$$

$$v_R=\hbar k_R/m_\perp. \tag{2.11b}$$

In all subsequent formulas we use spherical bands: $m_{||}=m_\perp=m$. Current conservation yields the unitarity of the collision matrix $\mathbf{u}$, given by

$$\mathbf{u}=\begin{bmatrix}u_{11} & u_{12}\\ u_{21} & u_{22}\end{bmatrix}. \tag{2.12}$$

In our problem, with no spin splitting of the spin-degenerate eigenstates, $\mathbf{u}$ is also symmetric. The electron density is readily obtained from Eqs. (2.6b), (2.10), and the unitarity of $\mathbf{u}$, to be

$$n^{(+)}(x)=n_R{}^{(+)}(x)\Theta(x)+n_L{}^{(+)}\Theta(-x), \tag{2.13a}$$

$$n_R{}^{(+)}(x)=\frac{2s+1}{4\pi^2}\int_0^{k_{FR}}dk_R\,[k_{FR}{}^2-k_R{}^2]$$
$$\times\{|\phi_{R-}(x)|^2+\mathrm{Re}[u_{22}\phi_{R+}{}^2(x)]\}, \tag{2.13b}$$

[21] See, e.g., R. G. Newton, J. Math. Phys. **1**, 319 (1960).
[22] See, e.g., I. Adawi, Phys. Rev. **146**, 379 (1966).

$$n_L^{(+)}(x)=\frac{2s+1}{4\pi^2}\int_\alpha^{k_{FL}} dk_L\,[k_{FL}^2-k_L^2]$$
$$\times\{|\phi_{L-}(x)|^2+\mathrm{Re}[u_{11}\phi_{L-}^2(x)]\}, \quad (2.13c)$$
$$k_{FR}^2=2m(\mu-V_0)/\hbar^2=k_{FL}^2-\alpha^2, \quad (2.14a)$$
$$k_{FL}^2=2m\mu/\hbar^2, \quad (2.14b)$$
$$\alpha^2=2mV_0/\hbar^2. \quad (2.14c)$$

The twofold "orbital" degeneracy of the continuum eigenstates for $E_x>V_0$ is reflected in Eqs. (2.13) by the fact that we have used the equality of $|\phi_+|^2$ and $|\phi_-|^2$ to extract a common factor of 2 in the two terms of (2.13b) and (2.13c).

In the energy region $0<E<V_0$, the eigenvalue spectrum is continuous but nondegenerate. The normalization condition (2.7a) gives for the wave function

$$\psi(x)=(2/\pi v_L\hbar)^{1/2}\,\mathrm{Re}[e^{i\delta}\phi_{L-}(x)]; \quad x<0 \quad (2.15a)$$
$$=(2\pi v_R\hbar)^{-1/2}V_{21}\phi_{R+}(x); \quad x>0$$
$$v_R\equiv\hbar q_R/m \quad (2.15b)$$

in which δ is a real phase shift of the reflected wave on the left-hand side of the barrier. The phase shift is determined from the equality of the logarithmic derivatives at $x=0$ to be

$$\delta=\tan^{-1}[N(E_x)/D(E_x)], \quad (2.16a)$$
$$N(E_x)=\mathrm{Re}[\phi_{L+}'(0)-L(E_x)\phi_{L+}(0)], \quad (2.16b)$$
$$D(E_x)=\mathrm{Im}[\phi_{L+}'(0)-L(E_x)\phi_{L+}(0)], \quad (2.16c)$$
$$L(E_x)=\phi_{R+}'(0)/\phi_{R+}(0). \quad (2.16d)$$

The "negative-energy" transition amplitude V_{21} is given by

$$V_{21}=2[k_Lq_R]^{1/2}\{[N^2+D^2]^{1/2}\phi_{R+}(0)\}^{-1}. \quad (2.17)$$

Equations (2.9), (2.16), and (2.17) permit the general proof of the relation (written for a step potential by Adawi[22]):

$$V_{21}^2(q_R,k_L)=|u_{21}(iq_R,k_L)|^2 \quad (2.18)$$

for all potentials of the form shown in Fig. 3 when $0<E_x<V_0$. If we further define

$$u_{11}\equiv e^{2i\delta(E)}, \quad (2.19)$$

then we can write the continuum contribution to the electron density as

$$n_c(x)=[n_R^{(+)}(x)+n_R^{(-)}(x)]\Theta(x)$$
$$+[n_L^{(+)}(x)+n_L^{(-)}(x)]\Theta(-x), \quad (2.20a)$$
$$n_R^{(-)}(x)=\frac{(2s+1)}{8\pi^2}\int_0^\alpha dq\,[k_{FR}^2+q^2]$$
$$\times|u_{21}(iq,k_L)|^2\phi_{R+}^2(x), \quad (2.20b)$$
$$n_L^{(-)}(x)=\frac{2s+1}{4\pi^2}\int_0^\alpha dk_L\,[k_{FL}^2-k_L^2]$$
$$\times\{|\phi_{L-}(x)|^2+\mathrm{Re}[u_{11}\phi_{L-}^2(x)]\}. \quad (2.20c)$$

For numerical computations, however, it is convenient to use densities obtained from (2.15a) directly, i.e.,

$$n_R^{(-)}(x)=\frac{(2s+1)}{2\pi^2}\int_0^\alpha dq_R\,[k_{FR}^2+q_R^2]$$
$$\times k_Lq_R[D^2(q_R)+N^2(q_R)]^{-1}$$
$$\times[\phi_{R+}(x)/\phi_{R+}(0)]^2, \quad (2.21a)$$
$$n_L^{(-)}(x)=\frac{(2s+1)}{2\pi^2}\int_0^\alpha dk_L(k_{FL}^2-k_L^2)$$
$$\times[D^2(k_L)+N^2(k_L)]^{-1}$$
$$\times[D(k_L)\,\mathrm{Re}\phi_{L-}(x)+N(k_L)\,\mathrm{Im}\phi_{L-}(x)]^2 \quad (2.21b)$$

in lieu of Eqs. (2.20). Finally, we find the expressions for the collision matrix in terms of the Jost functions:

$$u_{11}=[(k_L/k_R)^{1/2}\phi_{R+}(0)u_{21}-\phi_{L+}(0)]/\phi_{L-}(0), \quad (2.22a)$$
$$u_{22}=[(k_R/k_L)^{1/2}\phi_{L-}(0)u_{12}-\phi_{R-}(0)]/\phi_{R+}(0), \quad (2.22b)$$
$$u_{12}=u_{21}=\frac{2i(k_Lk_R)^{1/2}}{\phi_{R+}'(0)\phi_{L-}(0)-\phi_{R+}(0)\phi_{L-}'(0)}. \quad (2.22c)$$

The use of Eqs. (2.21) and (2.22) reduces the problem of calculating the continuum density $n_c(x)$ associated with a given potential $V(x)$ in (2.5b) to that of finding the Jost functions (2.8) and (2.9).

Equations (2.13), (2.20), (2.21), and (2.22) completely specify the local continuum density $n_c(x)$ as a functional of a local potential $V=V_d+V_{ec}$ occurring in Eq. (2.5a) and the chemical potential μ at zero temperature. The important consequences of these results are best illustrated by example in special cases. The remaining two parts of this section are devoted to this task.

C. The Step Potential

Although the exchange-correlation energy potentials play an important role in determining the interface potential, we might inquire for pedagogical reasons into the possibility of achieving a stable interface potential neglecting them entirely by using an initial model (step) potential

$$V(x)=V_0\Theta(x), \quad (2.23a)$$
$$V_0=E_{FL}-E_{FR}. \quad (2.23b)$$

The electron distribution associated with this potential has been studied by several authors[22–25] with emphasis on the asymptotic behavior as $x\to\infty$. The Jost functions are given for all x by their asymptotic forms (2.8)

[23] B. Dreyfus, R. Maynard, and A. Quattropani, Phys. Rev. Letters 13, 342 (1964).
[24] A. Bardasis, D. S. Falk, R. A. Ferrell, M. S. Fullenbaum, R. E. Prange, and D. L. Mills, Phys. Rev. Letters 14, 298 (1965).
[25] K. Yosida and A. Okiji, Phys. Rev. Letters 14, 301 (1965).

and (2.9) so that Eqs. (2.13) and (2.20) become

$$n_R(x)=n_R+\frac{(2s+1)}{4\pi^2}\int_0^{k_{FR}}[k_{FR}^2-k_R^2]dk_R \times\mathrm{Re}[u_{22}\,e^{2ik_Rx}]+\frac{2s+1}{8\pi^2}\int_0^{\alpha}dq_R\,[k_{FR}^2+q_R^2] \times|u_{21}(iq_R,k_L)|^2\,e^{-2q_Rx}, \quad (2.24a)$$

$$n_L(x)=n_L+\frac{(2s+1)}{4\pi^2}\int_0^{k_{FL}}dk_L\,[k_{FL}^2-k_L^2] \times\mathrm{Re}[u_{11}\,e^{-2ik_Lx}], \quad (2.24b)$$

$$n_R=(2s+1)k_{FR}^3/6\pi^2, \quad (2.25a)$$

$$n_L=(2s+1)k_{FL}^2/6\pi^2. \quad (2.25b)$$

In (2.24) and (2.25) we have chosen the chemical potential to be compatible with the bulk Fermi energies of the two sides of the interface. This selection is a consistent one due to (2.23b). As Eqs. (2.24) are valid for any potential of the form shown in Fig. 3, at sufficiently large $|x|$, we see that local charge neutrality at large distances from the junction is ensured by the above selection of chemical potential. For the step potential we also find

$$u_{22}=(k_R-k_L)/(k_R+k_L), \quad (2.26a)$$

$$u_{12}=2(k_Rk_L)^{1/2}/(k_R+k_L), \quad (2.26b)$$

$$u_{11}=(k_L-k_R)/(k_L+k_R);\ E>V_0$$

$$=\frac{k_L^2-q_R^2-2ik_Lq_R}{(k_L^2+q_R^2)};\quad 0<E<V_0. \quad (2.26c)$$

Using Eqs. (2.26) in (2.24) we can calculate the total integrated charge in the system. The result indicates that the tunneling charge $n_R^{(-)}(x)$ is exactly compensated by a loss of mobile charge in $n_L^{(-)}(x)$. It is an interesting fact that charge-neutrality is identically satisfied, despite the fact that the states $\psi_R^{(2)}(k_R=0, x)$ and $\psi_L^{(1)}(k_L=0, x)$ are zero for the step-well potential whereas they are unity for the respective infinite media. Other contributions to the charge density compensate for the loss of these states. These results demonstrate that the identification of E_{FR} and E_{FL} with the bulk Fermi energies yields both over-all charge neutrality as well as charge neutrality in the bulk of the two metals.[3]

In contrast to previous authors,[22–25] our primary interest is in the charge density close to the interface, not asymptotically far from it. We illustrate in Fig. 4 sample numerical evaluations of the integrals (2.24) using the collision matrix (2.26). The initial excess of negative charge on the low-density side of the junction is due to the tunneling (or "evanescent") term in (2.24a) whose integrand is proportional to $\exp(-2q_Rx)$. This term dominates the charge distribution in the region $0\leq x\lesssim k_{FT}^{-1}=(4k_{FR}/\pi a_B)^{-1/2}$ near the interface. The density in Fig. 4 is measured in units of a_B^{-3} with $a_B=(\hbar^2\epsilon/me^2)$ denoting the Bohr radius in the direction normal to the junction. As a_B can become quite large for small effective masses or large dielectric functions, the evanescent contribution in semimetals, degenerate semiconductors, and associated with small pieces of a Fermi surface in metals can extend over appreciable distances (~100 Å).

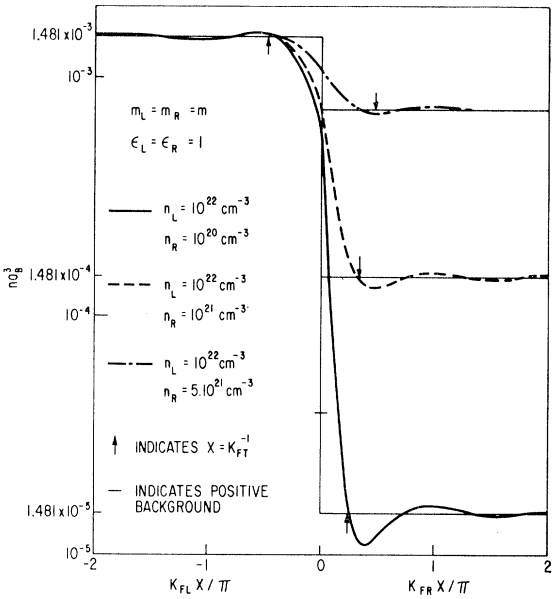

FIG. 4. The electron density in the nieghborhood of a bimetallic junction as calculated from a step model of the total electron potential chosen to equalize the Fermi energies of the two metals.

Far from the barrier all potentials give Friedel oscillations.[26] This result contrasts to the image-potential limit of a vacuum-metal interface at the vacuum side,[2,4] and makes a fully self-consistent model of the Poisson equation impossible in practice. From Fig. 4 we see that relatively little charge is contained in any but the first two regions of charge imbalance on either side of the interface. For the step potential the dipole layers in general yield a rising one-electron potential from the high- into the low-density metal. Therefore this model, incorporating direct Coulomb interactions alone, has the potentiality of yielding a self-consistent model of the interface. As such a model is not self-binding, we cannot use it to describe the dipole modifications of the work functions near a vacuum interface because, as discussed in the Introduction, the bulk separation energies dominate the work function.[2] Therefore we do not pursue this model potential any further.

D. The Step-Exponential Potential

An exactly solvable model potential of the general form shown in Fig. 3, which is an exponential potential

[26] J. Friedel, Advan. Phys. **3**, 446 (1954); Nuovo Cimento Suppl. **7**, 287 (1958).

like that obtained as the result of Fan's semiclassical analyses,[3] is given by (2.5b) with the selection

$$V_{ec}(x)=(-S_{nL}+E_{FL}-E_{FR}+S_{nR})\Theta(x), \quad (2.27a)$$

$$V_d(x)=\frac{-rV_d e^{h_L x}}{1+r}\Theta(-x) - V_d\left[1-\left(\frac{e^{-h_R x}}{1+r}\right)\right]\Theta(x), \quad (2.27b)$$

$$V_d=S_{nR}-S_{nL}, \quad (2.27c)$$

$$r=h_R/h_L\equiv\beta(n_R/n_L)^{1/6}. \quad (2.27d)$$

When $\beta=1$, the ratio r between the decay constants on the two sides of the interface is the ratio of their Fermi-Thomas wave numbers.

For the potential specified by Eqs. (2.27) the Jost functions are[10]

$$\phi_{L\pm}(x)=F(-Q_L^2, -h_L; \pm p_L, x), \quad (2.28a)$$

$$\phi_{R\pm}(x)=F(Q_R^2, h_R; \mp p_R, x), \quad (2.28b)$$

$$F(Q^2,h; p,x)=\exp(phx/2)\sum_{n=0}^{\infty}\left(\frac{Q^2 e^{-hx}}{h^2}\right)^n \times\frac{\Gamma(-p+1)}{n!\Gamma(n-p+1)}, \quad (2.28c)$$

$$Q_R^2=2mV_d/[\hbar^2(1+r)], \quad (2.28d)$$

$$Q_L^2=2mrV_d/[\hbar^2(1+r)], \quad (2.28e)$$

$$p_L=-i2k_L/h_L; \quad E_x>0 \quad (2.28f)$$
$$=2q_L/h_L; \quad E_x<0$$

$$p_R=-i2k_R/h_R; \quad E_x>V_0 \quad (2.28g)$$
$$=2q_R/h_R; \quad E_x<V_0.$$

The wave numbers k and q are defined in Eqs. (2.8) and (2.9). From (2.27) we see that as r becomes large, $h_R\gg h_L$ and $Q_L\gg Q_R$ so that the potential well on the left-hand side becomes both deeper and wider. It may then ultimately admit bound states (in the direction normal to the interface) which are associated with two-dimensional bands of states due to the continuum motion parallel to the interface.[17,18] The wave function of these states is

$$\psi_b(x)=C_L\phi_{L-}(x)\Theta(-x)+C_R\phi_{R+}(x)\Theta(x) \quad (2.29a)$$

and their eigenvalue equation is

$$\frac{F'(-Q_L^2-h_L; -p_L, 0)}{F(-Q_L^2, -h_L; -p_L, 0)}=\frac{F'(Q_R^2, h_R; -p_R, 0)}{F(Q_R^2, h_R; -p_R, 0)}. \quad (2.29b)$$

The normalization criterion (2.7b) gives

$$C_L=\gamma_{LR}C_R, \quad (2.30a)$$

$$C_R^2=[I_1+\gamma_{LR}^2 I_2]^{-1}, \quad (2.30b)$$

$$\gamma_{LR}=F(Q_R^2, h_R; -p_R, 0)/\times F(-Q_L^2-h_L; -p_L, 0), \quad (2.30c)$$

$$I_1=\int_0^{\infty} dx\,|F(Q_R^2, h_R; -p_R, x)|^2, \quad (2.30d)$$

$$I_2=\int_{-\infty}^{0} dx\,|F(-Q_L^2, -h_L; -p_L, x)|^2. \quad (2.30e)$$

The continuum electron density is obtained by using Eqs. (2.28) in Eqs. (2.22), (2.20), and (2.13).

From Eqs. (2.27) we see that as the width of the potential on the high-density side ($1/h_L$) increases, the fraction of the total voltage drop V_d across the left-hand side increases for fixed h_R. Therefore by taking a fixed value of h_R and increasing h_L we make the left-hand potential wider and deeper while making the right-hand potential more shallow. Taking the Fermi-Thomas values for h_L and h_R, the left-hand potential well does not bind a state with $E<0$ for $n_L=10^{22}$ and $n_R=10^{21}$ cm^{-3}. The one-electron charge density, and the model density with which it is approximated in the self-consistent calculation, are shown in Fig. 5. Two aspects of the figure are significant. First, in the absence of the localized states, most of the deviations from charge neutrality occur in the two oscillations of $n_e(x)$ about n_p immediately adjacent to the boundary at $x=0$. Thus a "four-region" model of the charge density as shown on the figure suffices to parametrize the calculated density in the self-consistency calculation to be described in the next section. The second important feature of the figure is the concentration of the charge in the positive-charge oscillation labeled I in the figure. Most of the voltage drop V_d occurs across this region which corresponds to the classical depletion region of a Schottky-barrier model of the junction. However, the semiclassical Schottky description of regions I and II

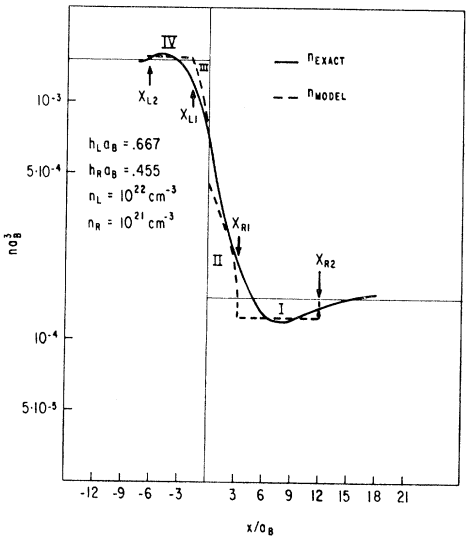

FIG. 5. The actual electron density and model electron density in the neighborhood of a bimetallic junction as calculated from the starting potential used in the iteration procedure. The total electron potential was taken equal to the sum of the bulk exchange-correlation potential in each metal and an exponential dipole potential [Eq. (2.27)].

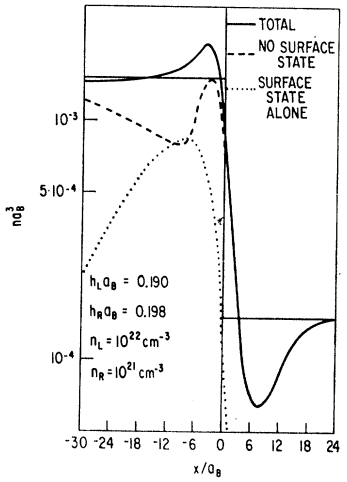

FIG. 6. The electron density in the neighborhood of a bimetallic junction when a single surface state is present.

near the interface is completely inadequate because of the evanescent contribution to the charge on the low-density side. This contribution to $n_e(x)$, due to the tunneling of electrons into the low-density side of the junction, causes the negative-charge excess in region II as well as the fact that the positive-charge excess never exceeds one-third of its maximum possible (i.e., classical) value. In the self-consistent potential described in the next section the positive-charge excess reaches four-fifths of its classical value.

The influence of a bound state with $E_x<0$ is shown in Fig. 6. The parameters associated with the potential leading to the illustrated charge density are chosen to give a single bound state at $p_L=i(0.377)$ which is almost the maximum binding possible before a second bound-state appears. For less tightly bound states the associated charge density is less well localized near the interface. This bound state for motion normal to the interface gives rise to a two-dimensional band of states due to the continuum motion parallel to the interface. Such bound states may have been observed in tunneling[17] experiments in semimetals and in transport[14–16] and optical absorption[18] experiments in degenerate surface layers on semiconductors. These states, while not directly analogous to the Tamm or Shockley states,[11] because they are not associated with the breaking of the translational symmetry of a crystal lattice, are calculated by matching wave functions in a manner which is equivalent to the use of the effective-mass approximation[10] in Heine's[12] method of finding "virtual" surface states. However, we emphasize that if such states occur for a particular set of parameters in our model, they must be dynamically stable in that their charge is explicitly incorporated in calculating the potential in which they are bound. This requirement stands in contrast to the conventional calculations[11,12] in which filling the surface states with electrons leads to a modified potential in which the states may no longer exist.

Summarizing the results of our two model calculations of the electron density, we have shown that in the absence of surface states a four-region model of the charge fluctuations near the interface adequately approximates the calculated density. Surface two-dimensional energy bands can occur, and are associated with rather extended charge distributions even for "metallic" bulk electron densities. A Schottky-barrier model of the junction is inadequate because it neglects the evanescent contribution to the charge density caused by electrons tunneling into the low-density electron gas. The full self-consistent determination of the junction potential is discussed in the next section.

III. SELF-CONSISTENT CALCULATION OF THE JUNCTION POTENTIAL

A. The Model Charge Density

As indicated in Sec. IIA, the major task in a self-consistent treatment of the interface is the establishment of a model of the charge density which guarantees charge neutrality and the proper dipole potential V_d at each step of the self-consistent iteration process. These requirements dictate use of a model expression to approximate the numerical charge density because the accuracy required to obtain reliable asymptotic values for the Friedel oscillations necessitates excessive computing time on the electronic computer (GE 235) which we used. Poisson's equation (2.1) need not be analytically solvable for the model charge density, but for convenience in determining the proper V_d we use models for which $V_d(x)$ can be obtained in closed form in terms of the parameters of the model density function.

For the charge density either with or without surface-state bands we use a four-region model charge density given by

$$\begin{aligned} n_M(x)&\equiv n_p(x)-n_e(x)\\ &=-n_{L2}; && -x_{L2}\leq x\leq -x_{L1}\\ &=n_{L1}(1+x/x_{L1}); && -x_{L1}\leq x\leq 0\\ &=-n_{R1}(1-x/x_{R1}); && 0\leq x\leq x_{R1}\\ &=n_{R2}; && x_{R1}\leq x\leq x_{R2}\\ &=0; && \text{otherwise}. \end{aligned} \tag{3.1}$$

This model contains eight parameters $\{n_{Li}, x_{Li}, n_{Ri}, x_{Ri}; i=1, 2\}$ of which only six are independent due to the requirements that the total dipole potential is V_d and that both $V_d(x)$ and $V_d'(x)$ be continuous. The solution to Poisson's equation (2.1) using the model charge density (3.1) is

$$\begin{aligned} V_d(x)&=-V_{L1}^{(2)}(1+x/x_{L2})^2; && -x_{L2}\leq x\leq -x_{L1}\\ &=-V_{Ld}^{(2)}\left[1+\frac{2x}{(x_{L1}+x_{L2})}\right]\\ &\quad+V_L^{(1)}\left[\frac{1}{3}\left(\frac{x}{x_{L1}}\right)^3+\left(\frac{x}{x_{L1}}\right)^2+\left(\frac{x}{x_{L1}}\right)+\frac{1}{3}\right]; && -x_{L1}\leq x\leq 0 \end{aligned} \tag{3.2a}$$

$$= -V_d + V_{Rd}^{(2)}\left[1 - \frac{2x}{(x_{R1}+x_{R2})}\right] + V_R^{(1)}\left[\frac{1}{3}\left(\frac{x}{x_{R1}}\right)^3 - \left(\frac{x}{x_{R1}}\right)^2 + \left(\frac{x}{x_{R1}}\right) - \frac{1}{3}\right]; \quad 0 \le x \le x_{R1}$$

$$= -V_d + V_R^{(2)}\left[\frac{x}{x_{R1}} - 1\right]^2; \quad x_{R1} \le x \le x_{R2};$$

$$\begin{aligned} V_L^{(1)} &= 2\pi n_{L1} e^2 x_{L1}^2/\epsilon_L, \\ V_L^{(2)} &= 2\pi n_{L2} e^2 x_{L2}^2/\epsilon_L, \\ V_{Ld}^{(2)} &= 2\pi n_{L2} e^2 (x_{L2}^2 - x_{L1}^2)/\epsilon_L; \end{aligned} \tag{3.2b}$$

$$\begin{aligned} V_R^{(1)} &= 2\pi n_{R1} e^2 x_{R1}^2/\epsilon_R, \\ V_R^{(2)} &= 2\pi n_{R2} e^2 x_{R2}^2/\epsilon_R, \\ V_{Rd}^{(2)} &= 2\pi n_{R2} e^2 (x_{R2}^2 - x_{R1}^2)/\epsilon_R. \end{aligned} \tag{3.2c}$$

The continuity of V_d and V_d' at $x=0$ gives the two constraints

$$V_d = -\tfrac{1}{3}(V_R^{(1)} + V_L^{(1)}) + (V_{Rd}^{(2)} + V_{Ld}^{(2)}), \tag{3.3a}$$

$$2V_{Rd}^{(2)}(x_{R1}+x_{R2})^{-1} - 2V_{Ld}^{(2)}(x_{L1}+x_{L2})^{-1} = V_R^{(1)} x_{R1}^{-1} - V_L^{(1)} x_{L1}^{-1}. \tag{3.3b}$$

We further constrain the parameters by the requirements that (a) x_{L2} and x_{R2} are chosen to be at the half drop-off values of the charge deviations from the maximum deviations of regions IV and I (Fig. 5). (b) The four model charge densities n_{R1}, n_{R2}, n_{L1}, and n_{L2} are obtained from the calculated charge density $n(x)$ by the procedure of: (1) Select x_{L1} and x_{R1} to be the smallest values of $|x|$ on either side of the junction at which $n(x)=0$, (2) using these values, and those of x_{L2} and x_{R2} given by constraint (a), calculate the values of n_i so that in each of the four regions of the model charge density, the integrated charge density equals the integrated charge density of the corresponding region in $n(x)$, and (3) after the model n_i are chosen, treat x_{R1} and x_{L1} as variable parameters which are determined from the two conditions (3.3) for charge neutrality and the proper dipole voltage drop across the interface.

The above fitting procedure is carried out in each step of the self-consistent iteration procedure.

B. Application of the Self-Consistency Criteria

In Sec. IIA we found that a self-consistent-field calculation required the solution of two differential equations [Poisson's Eq. (2.1) and Schrödinger's Eq. (2.5)] and the performance of one quadrature to obtain the electron density from the solutions to the Schrödinger equation. The numerical performance of the quadrature seems unavoidable although by use of an appropriate model charge density in the model approximation to the numerical result one can analytically solve both of the differential equations [e.g., an array of step functions for $n(x)$ and Weber-function wave functions[10]]. Unfortunately, the charge densities of Figs. 5 and 6 cannot be accurately parametrized by model charge densities for which the solution $V_d(x)$ to Poisson's equation (2.1) leads to an analytically solvable Schrödinger equation (2.5). However, the discussion in Sec. III A indicates that although the charge densities must be parametrized by charge-neutral model densities, models for which Poisson's equation is solvable are adequate for our purposes. Therefore the numerical analysis is reduced to the solution of Schrödinger's equation (2.5) and the superposition of these solutions to compute the electron densities via Eq. (2.6) and its subsequent extensions (2.13), (2.21), and (2.22).

The computer program used to perform the numerical work is described in Appendix A. Numerical calculations were performed first for a system in which the high-density metal was characterized by $n_L = 10^{22}$ cm^{-3} and the low-density metal by $n_R = 10^{21}$ cm^{-3}. The starting potential $V_d(x)$ is taken to be the step exponential (discussed in Section II D) with decay lengths h_R and h_L given by their Thomas-Fermi values. Figure 5 shows the calculated charge density and the model charge density determined as described in the preceding section. The potential due to the model charge density was used in the first iteration. The resulting charge density together with the fitted-model charge density is shown in Fig. 7. The charge densities found in the third and fourth steps of the iteration together with their associated model charge densities, are shown in Figs. 8 and 9, respectively. Since the difference in the calculated charge densities shown in these two figures is reasonably small, i.e., as compared to the difference in the densities of Figs. 7 and 9, the iteration was terminated. One consequence

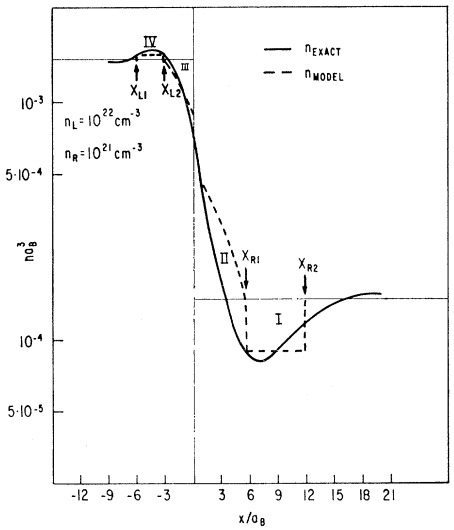

FIG. 7. The actual electron density and model electron density in the neighborhood of a bimetallic junction as calculated in the first iteration (Sec. III B).

of our simplified four-region model is that the final model charge density is not a particularly good representation of the calculated charge distribution. However, the general character of the potentials associated with the two distributions is similar. Figure 10 shows the potentials used to calculate the densities found in first, second, fourth, and fifth steps of the iteration. The figures indicate that the size of the depletion region in the low-density metal increases significantly as self-consistency is approached, so that the self-consistent potential gives a depletion region more like a Schottky barrier than the starting potential.

The most important aspect of the above results is that the self-consistent procedure does "converge" to give a final potential shown in Fig. 10 of the form illustrated in Fig. 3. A self-consistent procedure is essential to determine the details of the junction potential because only such a procedure determines the "decomposition" of the voltage drop V_d between the two sides of the interface. An interesting feature of the final potential is the attainment of its maximum value to the right of the junction. Because of this fact, the final barrier height satisfies Eq. (1.4) in which the equality is almost relevant: $V_b \cong V_d$. The shift in the maximum of $V_d(x)$ for the four-region model to $x_m > 0$ is the cause of the comment above Eq. (1.4) that this relation was "probably" satisfied. It is possible, although we have not found such a case, that $V_b > V_d$ for a dipole potential $V_d(x)$ of the final forms shown in Fig. 10.

We recall from the Introduction that the case $n_R = 10^{21}$ cm^{-3} and $n_L = 10^{22}$ cm^{-3} is typical of electron densities below 10^{22} cm^{-3} in that the lower-density electron gas exhibits a smaller magnitude $|Sn|$ of the separation energy. The range of values of n for the Group-I metals, which are most nearly free-electron metals, is from $n = 0.85 \times 10^{22}$ cm^{-3} (Cs) to 8.5×10^{22} cm^{-3} (Cu). Therefore to the extent that the free-electron gas model correctly gives the bulk metallic separation energies, most bimetallic junctions are composed of metals for which the higher-electron-density metal exhibits a smaller magnitude $|Sn|$ of the separation energy. For such junctions the sign of the dipole potential step across the interface is reversed from that

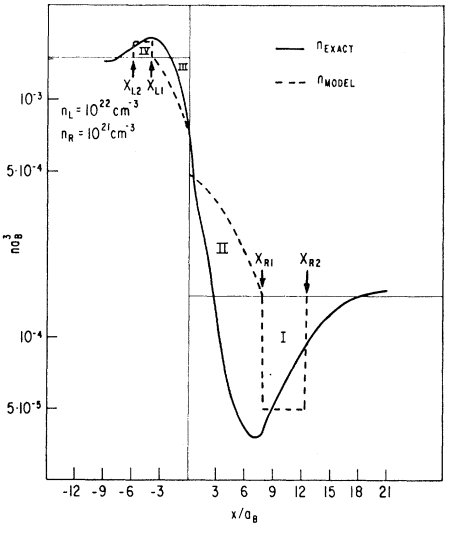

FIG. 8. The actual electron density and model electron density in the neighborhood of a bimetallic junction as calculated in the third iteration (Sec. III B).

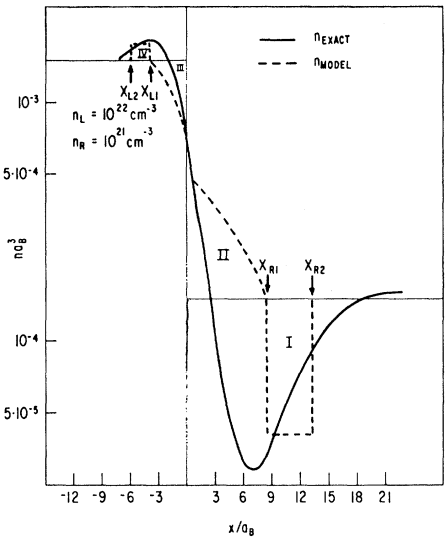

FIG. 9. The actual electron density and model electron density in the neighborhood of a bimetallic junction as calculated in the fourth (last) iteration (Sec. III B).

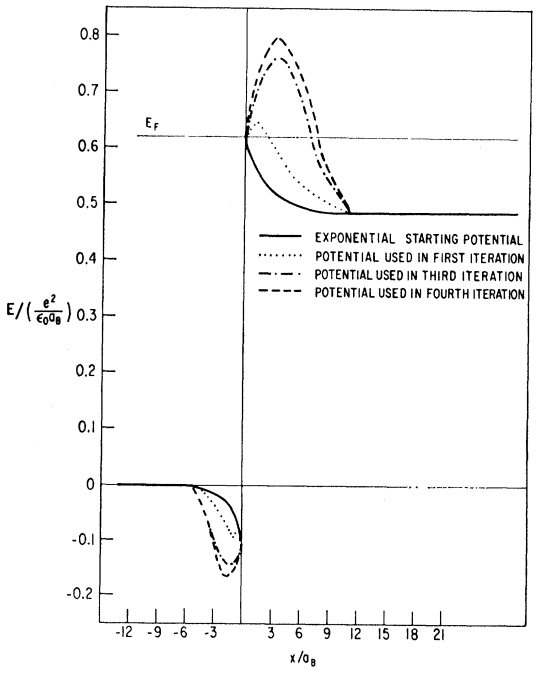

FIG. 10. The starting potential and the potentials used to calculate the electron density in the first, third, and fourth iterations.

shown in Figs. 2 and 3. A two-region model of the charge density presumably can describe adequately the dipole effects at these junctions. In the four-region model, regions II and III, rather than I and IV as in Figs. 7–9, dominate the dipole potential. We have performed a set of calculations parallel to those illustrated in Figs. 7–10 for $n_L=5\times10^{22}$ cm^{-3} and $n_R=10^{22}$ cm^{-3}. Self consistency in our rough sense can be achieved also in this case using the four-region-model charge density. The case of $n_L=10^{22}$ cm^{-3} and $n_R=10^{21}$ cm^{-3} provides a more stringent test of the model, however, and hence has been discussed in more detail. Although the dipole contribution to the junction potential exhibits a net sign difference in the two cases, the total junction potentials are qualitatively similar.

C. Discussion

Our primary objectives in this study were the construction of a "first-principles" model of a bimetallic interface and its subsequent application to explore the role of the electrostatic charge density in determining the one-electron ("junction") potential at the interface. Although often mentioned in passing, the contribution to the junction potential of the modification of the bulk electrostatic charge densities of the two components at their common interface has not been investigated in detail prior to this analysis. For what appear to be historical reasons,[1,11,12] the phenomenological approach to junction potentials,[1,8,11] especially at metal-semiconductor contacts, has emphasized constructs employing entirely *ad hoc* distributions of localized surface charge introduced for the sole purpose of making the experimental data compatible with Eq. (1.1), and the observed insensitivity of the barrier height V_b to a (constant) bias applied across the junction. The inapplicability of such constructs for the description of intimate metal-semiconductor contracts was recognized by Heine[12] who applied the nearly-free-electron model to describe both the metal and semiconductor and emphasized the role of the evanescent electron density as the proper quantum-theory replacement for the phenomenological construct of surface charge. We have added two new considerations to those of Heine.[12] First, we have shown that the difference in the bulk cohesive energies of the two components of the junction dictates the qualitative features of the junction potential and thereby the general character of the charge distribution near the interface. Second, by adopting a model in which the bulk cohesive energy is calculable, we have been able to explore in detail the role of the electrostatic charge redistribution near the interface in determining a self-consistent junction potential from which the charge distribution is itself determined.

The most significant results of our analysis are: (a) The determination that the charge distribution near the junction has the "four-region" character shown in Figs. 5–9, and (b) the verification that using such a "four-region" model of the charge density a rough self-consistency between the charge-density and its concommitant junction potential can be achieved in the sense of Sec. III B. Surface states, either conventional[11] or of the "localized-state" variety discussed in Sec. II, are conspicuous by their absence in the final self-consistent charge density for our example of $n_L=10^{22}$ and $n_R=10^{21}$ cm^{-3}. As these values of n_L and n_R were chosen to give a large dipole potential difference V_d in the opposite sense to that caused by a simple two-region charge density, the absence of surface states for this special example strongly suggests that their absence is the rule and their presence is the exception. If, following Heine,[12] we were to take a free-electron model of the semiconductor at a metal-semiconductor contact, the density difference between the electron fluid in the metal and semiconductor would almost always be less than the factors of 10 and 5, respectively, used in the calculations described in the previous section. In this respect our analysis strengthens Heine's conclusion that conventional surface states do not occur in the absence of band bending to the much stronger result that in our model localized states are dynamically unstable for the (limiting) cases of large Δn and V_d. Therefore, the introduction of localized states in a phenomenological description of the junction potential would be both unnecessary and incorrect. The burden of determining the junction potential is absorbed entirely by the local modifications of the electronic density. In particular, the considerable band bending evident in Fig. 10 does not require the introduction of localized "surface" states.

In conclusion, we reiterate the limitations of the analysis and give our assessment of the significance of these limitations. Independent of questions concerning the validity of the model, in this paper we have not fully explored its consequences because of our neglect of the spatial and momentum (energy) dependence of the exchange and correlation potential. Self-consistent calculations of the junction potential using the local-density (Fermi-Thomas) approximation[7] for the exchange-correlation potential have been carried out. They lead to qualitatively the same results but with larger depletion regions and will be reported on elsewhere.[27] As the local-density approximation overestimates the effects of the exchange-correlation energy,[4] we believe that the qualitative features of the results given in this paper accurately characterize the predictions of our jellium model of the junction.

The major limitation of the model itself is its failure to incorporate the background of positive charge as an appropriate array of positive-ion cores rather than a uniform charge density. Furthermore, the inclusion of the ion-core effects must be done in such a way as to yield reasonable results for the bulk cohesive energy of the composite materials of the junction. This require-

[27] A. J. Bennett and C. B. Duke (to be published).

ment already eliminates the systematic use of a simple nearly-free-electron model as a "first-principles" model of a metal-semiconductor contact due to the difficulty in calculating the cohesive energy of the semiconductor.[9] Thus in applying an extended version of the model to semiconductors, a phenomenological energy shift probably must be introduced in order to give the bulk cohesive energy. As we do not yet have experience in dealing with such an extended model, we can only conjecture that as a high-energy electron in a semiconductor can be described by a nearly-free-electron model, the photoemission or thermionic-emission barrier heights at metal-semiconductor contacts may be adequately predicted by the jellium model with appropriate adjustments to give the observed bulk cohesive energy of the semiconductor. The description of the properties of low-energy electrons (e.g., Ohmic-contact tunneling experiments) obviously requires at least a two-band treatment of the periodic potential in the semiconductor.

A second limitation of the model is its suitability only for the description of the equilibrium junction potential at the interface. The validity of the (nearly-) free-electron model to describe the interface rests fundamentally on the invariance of the partition function of the total system on the selection of eigenfunction representation used to evaluate it.[12] If, for example, a bias is imposed across the junction, then current begins to flow and a detailed consideration of the scattering mechanisms limiting this flow becomes necessary in order to establish the junction potential. At a bimetallic interface between nearly-equal-density metals, no space-charge depletion region occurs in the low-density metal and bulk transport effects materially alter the character of the junction potential. If a depletion region occurs on the low-density (right-hand) side, then, for example, when a bias $eV \ll V_b - E_{FR}$, is applied to the junction, the current flow is limited by tunneling through the space-charge barrier so that the alterations in the charge density, and hence junction potential, are small (but not necessarily negligible).[10]

Summarizing, we have constructed a "first-principles" jellium model of a bimetallic interface and demonstrated the model's prediction that the self-consistent junction potential is usually due to redistribution of the (continuum) electron density and not to localized surface charge. The model is applicable for the calculation only of the equilibrium junction potential. Quantitative expressions for nonequilibrium corrections to the junction potential are not derived.

ACKNOWLEDGMENTS

One of us (CBD) would like to thank Dr. P. L. Read for a series of stimulating discussions on interface potentials during which the problem solved in this paper originally was formulated.

APPENDIX A: NUMERICAL EVALUATION OF THE ELECTRON DENSITY

The numerical evaluation of the electronic density consists of solving the Schrödinger equation and then integrating [Eqs. (2.6)] over the densities associated with the various filled electronic states. The particular solutions which are required in Eqs. (2.6) are those whose asymptotic behavior is given by Eqs. (2.10) and (2.15). The limits of integration of the Schrödinger equation, $x = L_2$ and $x = -L_1$, are chosen such that the potential at those points is flat (in the case of the model parabolic potential) or negligibly varying (in the case of the model exponential potential). The different energy regions are treated as follows:

Case (a): $0 < E < V_0$. The integration of the wave equation (2.5) is begun at $x = L_2$, where it is assumed that

$$\psi(L_2) = \phi_{R+}(L_2), \tag{A1}$$

and continued to $x = -L_1$, where the wave function obtained is given by

$$\psi(-L_1) = A \operatorname{Re}[e^{i\delta}\phi_{L-}(-L_1)]. \tag{A2}$$

A and δ are determined from the derivative and value of the calculated function which is then multiplied by $(2/\pi v_L \hbar)^{1/2} A^{-1}$ to give the correct asymptotic forms (2.15).

Case (b): $V_0 < E < E_F$. The function $\psi^{(1)}(x)$ is determined by assuming a starting value at $x = L_2$ of

$$\psi^{(1)}(L_2) = \phi_{R+}(L_2) \tag{A3}$$

and integrating to $x = -L_1$, where $\psi^{(1)}(-L_1)$ is given by

$$\psi^{(1)}(-L_1) = A[\phi_{L+}(-L_1) + u_{11}\phi_{L-}(-L_1)]. \tag{A4}$$

The quantities u_{11} and A are determined from the derivative and value of the calculated function which is then renormalized to give the correct asymptotic forms (2.10).

The function $\psi^{(2)}(x)$ is obtained in a similar way; the integration being begun at $x = -L_1$ and continuing to $x = L_2$.

The accuracy of the numerical integration of the Schrödinger equation was checked by comparing the calculated wave function with those obtained analytically for the two solvable potentials of Secs. II C. and II D. The convergence of the integral (2.6) was at all times better than 1%. In addition, the asymptotic values of the electronic density associated with the step potential agreed with those obtained analytically.